University of Reading

On the anticorrelation between H3+ temperature and density in giant planet ionospheres

Article

Published Version

Open Access

Melin, H., Stallard, T. S., O'Donoghue, J. ORCID: https://orcid.org/0000-0002-4218-1191, Badman, S. V., Miller, S. and Blake, J. S. D. (2014) On the anticorrelation between H3+ temperature and density in giant planet ionospheres. Monthly Notices of the Royal Astronomical Society, 438 (2). pp. 1611-1617. ISSN 1365-2966 doi: 10.1093/mnras/stt2299 Available at https://centaur.reading.ac.uk/120102/

It is advisable to refer to the publisher's version if you intend to cite from the work. See Guidance on citing.

To link to this article DOI: http://dx.doi.org/10.1093/mnras/stt2299

Publisher: Oxford University Press

All outputs in CentAUR are protected by Intellectual Property Rights law, including copyright law. Copyright and IPR is retained by the creators or other copyright holders. Terms and conditions for use of this material are defined in the End User Agreement.

www.reading.ac.uk/centaur

University of Reading

CentAUR

Central Archive at the University of Reading

Reading's research outputs online

Monthly Notices
of the
ROYAL ASTRONOMICAL SOCIETY

MNRAS **438,** 1611–1617 (2014)
Advance Access publication 2013 December 21

doi:10.1093/mnras/stt2299

On the anticorrelation between H_3^+ temperature and density in giant planet ionospheres

H. Melin,[1,2⋆] T. S. Stallard,[1] J. O'Donoghue,[1] S. V. Badman,[3] S. Miller[4] and J. S. D. Blake[1]

[1]*Department of Physics & Astronomy, University of Leicester, University Road, Leicester LE1 7RH, UK*
[2]*Space Environment Technologies, 1676 Palisades Dr., Pacific Palisades, CA 90272, USA*
[3]*Department of Physics, University of Lancaster, Lancaster LA1 4YW, UK*
[4]*University College London, Gower Street, London WC1E 6BT, UK*

Accepted 2013 November 27. Received 2013 November 27; in original form 2013 October 4

ABSTRACT

The intensity of H_3^+ emission can be driven by both temperature and density, and when fitting a set of infrared H_3^+ line spectra, an anticorrelation between the fitted temperatures and densities is commonly observed. The ambiguity present in the existing published literature on how to treat this effect puts into question the physical significance of the derived parameters. Here, we examine the nature of this anticorrelation and quantify the inherent uncertainty in the fitted temperature and density that this produces. We find that the uncertainty produced by the H_3^+ temperature and density anticorrelation is to a very good approximation equal to the uncertainties that are derived from the fitting procedure invoking Cramer's rule. This means that any previously observed correlated variability in the observed H_3^+ temperature and density outside these errors, in the absence of other error sources, are statistically separated and can be considered physical. These results are compared to recent ground-based infrared Keck Near InfRared echelle SPECtrograph (NIRSPEC) observations of H_3^+ emission from Saturn's aurora, which show no clear evidence for large-scale radiative cooling, but do show stark hemispheric differences in temperature.

Key words: planets and satellites: atmospheres – planets and satellites: aurorae – planets and satellites: gaseous planets – planets and satellites: magnetic fields.

1 INTRODUCTION

The infrared spectrum of the very simplest molecular ion, H_3^+, was first observed in the laboratory by Oka (1980) and has since been used as a valuable tool to the study physical conditions of both the upper atmospheres of the giant planets (Drossart et al. 1989), molecular clouds (McCall et al. 1999) and the interstellar medium (Geballe & Oka 1996). It is formed very efficiently via the ionization of H_2, and H_3^+ produced in these environments reveals the injection of energy sufficient to ionize atomic and molecular hydrogen. This energy is generally either in the form of ultraviolet radiation or energetic particles (Miller et al. 2000, 2006). By analysing the H_3^+ ν_2 ro-vibrational P, Q and R branches of the spectrum (defined by change in rotational quantum number, $\Delta J = 1$, 0, and -1, respectively), one can derive both the temperature and density of the emitting ions. In conditions of local thermodynamic equilibrium (LTE), the H_3^+ ion temperature is equal to the temperature of the surrounding neutrals, which in the case of a planetary atmosphere means that the ionospheric H_3^+ temperature is equal to the thermospheric temperature. Thus, we can use ground-based IR observations of H_3^+ emission from astrophysical sources to determine the physical properties of the medium in which these ions are emitting (Miller et al. 2006).

Emission from H_3^+ was discovered at the polar regions of Jupiter by Drossart et al. (1989), and is observed to have temperatures ranging between 800 and 1200 K (Lam et al. 1997; Stallard et al. 2002). These high temperatures are driven by the large-scale magnetospheric currents that inject energy, mainly in the form of Joule heating (Cowley & Bunce 2003; Melin et al. 2006). In contrast, the temperature of Saturn's auroral ionosphere was determined to be much cooler than that of Jupiter, at 450 ± 50 K (Melin et al. 2007). More recent observations by Melin et al. (2011a), Stallard et al. (2012) and O'Donoghue et al. (2014) yielded higher temperatures at Saturn, between 500 and 600 K. In addition to the auroral component of H_3^+, it is also produced across the entire disc of the planet, generated by solar ionization of molecular hydrogen (Stallard et al. 2012; O'Donoghue et al. 2013).

The H_3^+ temperature at Uranus is seen to vary over very long timescales, cooling from ∼740 K in 1992 to ∼530 K in 2011 (Melin et al.

⋆ E-mail: h.melin@ion.le.ac.uk

© 2013 The Authors
Published by Oxford University Press on behalf of the Royal Astronomical Society

Downloaded from https://academic.oup.com/mnras/article/438/2/1611/1013156 by guest on 06 May 2025

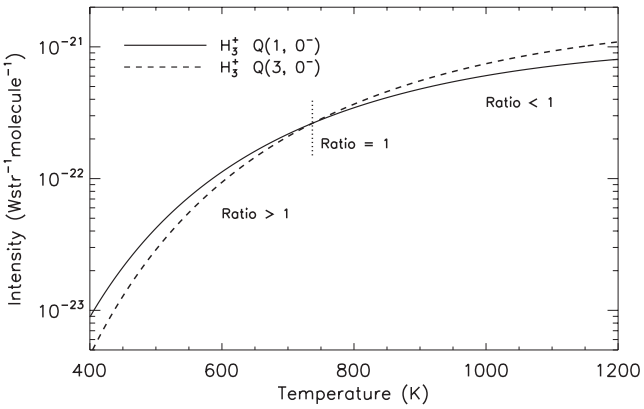

Figure 1. The intensity of the H_3^+ $Q(1, 0^-)$ at 3.953 μm (solid) and H_3^+ $Q(3, 0^-)$ at 3.986 μm (dashed) lines as a function of temperature. The two lines evolve at different rates, and the ratio of the two can be used a proxy for the temperature. The dotted line indicates where the ratio of the two lines is equal to 1, occurring at a temperature of 737 K.

2011c, 2013), suggesting either a seasonal or long-term magnetospheric control of the thermal state of its upper atmosphere. The mechanism that controls these temperatures remains poorly understood.

H_3^+ emissions from Neptune remain undetected (Feuchtgruber & Encrenaz 2003; Melin et al. 2011b), suggesting an anomalously rarefied H_3^+ ionosphere. This is surprising, as Voyager 2 observed ∼few × 10^9 m^{-3} peak electron densities at both Uranus (Tyler et al. 1986) and Neptune (Tyler et al. 1989). This may mean that H_3^+ is not an important constituent of the ionosphere at Neptune, perhaps being quenched by hydrocarbons extending high into the thermosphere (Melin et al. 2011b).

The differences in intensity of the H_3^+ emission observed at Earth from Jupiter, Saturn, and Uranus are driven mainly by temperature. Fig. 1 shows that the intensity of the *Q*-branch emission of H_3^+ increases at an exponential rate as the temperature increases. For example, the intensity of the H_3^+ $Q(1, 0^-)$ transition at 1000 K is 14 times more intense than at 500 K, as illustrated in Fig. 1. Hence, the observed intensity of H_3^+ is driven both by temperature (exponentially) and the number of ions that are emitting (linearly) – this is explored in more detail in Section 3. The confidence with which the parameters can be determined is governed principally by the fidelity of the observed spectrum – parametrized by the signal-to-noise ratio (SNR).

An anticorrelation between the fitted H_3^+ temperature and density has been noted by Lam et al. (1997) and Raynaud et al. (2004), both of whom analysed auroral emission from Jupiter. They noted for a particular fit, the range of possible temperatures and densities is potentially large, such that the anticorrelation introduces larger uncertainties than the statistics of the spectral fit would suggest. If this assessment is correct, what is the appropriate method by which to assign uncertainties to these parameters? In other words, when do we become 'certain' that our uncertainties are large enough?

There is also an argument to be made that the H_3^+ temperature and density anticorrelation is actually a real physical effect – this is known as the H_3^+ *thermostat* (Miller et al. 2010). If a region in the ionosphere contains more H_3^+ ions than another region (at the same temperature), it radiates more IR energy to space, which has the effect of cooling the surrounding thermosphere. In such a way, we may expect high-density regions to be cooler than low-density regions. This effect has been shown to be very important for extrasolar planets that orbit close to their parent star (Koskinen, Aylward & Miller 2007). We may also expect an anticorrelation to exist if different altitude of the ionosphere are sampled, with high-altitude regions being hotter and less dense, while low-altitude regions are cooler and more dense (e.g. Lystrup et al. 2008).

The ambiguity in the published literature regarding how to treat, and trust, the errors on the H_3^+ temperature and column-integrated density enforces the need to quantify this in some detail. Both Lam et al. (1997) and Raynaud et al. (2004) identified the interdependence of these two parameters, giving rise to an apparent anticorrelation when analysing a set of H_3^+ spectra with modest SNR. Both of these studies used a least-squares fitting routine to derive the H_3^+ parameters by minimizing the difference between the observed and modelled theoretical spectra (see Section 3).

Here, we fit a large set of synthetic H_3^+ spectra at known temperatures and densities, for a wide range of SNRs, to investigate if the effects of the H_3^+ temperature and density anticorrelation produce larger physical uncertainties than those produced by the fitting process. We then apply these findings to Keck Near InfRared echelle SPECtrograph (NIRSPEC) observations of Saturn's polar ionosphere.

2 KECK OBSERVATIONS

Recently, the analysis of IR Keck NIRSPEC (McLean et al. 1998) observations of H_3^+ emission from the northern and southern auroral regions of Saturn presented by O'Donoghue et al. (2014) show a clear anticorrelation between the fitted temperature and column integrated density between separate observations. With relatively modest SNR – about 20 – the range of possible temperature and density values a particular spectrum can assume is large, and the two parameters are highly anticorrelated. This is seen in Fig. 2, showing the fitted H_3^+ temperatures for each hemisphere as a function column-integrated densities (from table 1 in O'Donoghue et al. 2014). The fitting routine is described in more detail in Section 3.

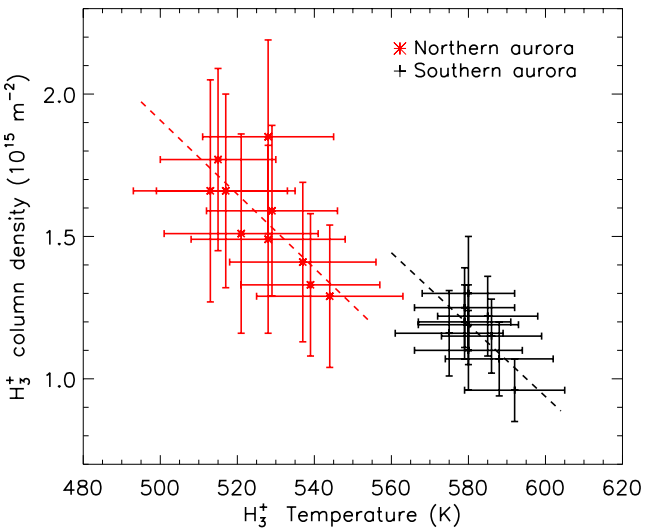

Figure 2. The H_3^+ temperature and density derived from Keck NIRSPEC observations of Saturn's northern (stars) and southern (crosses) aurora from the 2013 April 17 (O'Donoghue et al. 2014). The Pearson correlation coefficient between temperature and density for the northern aurora is −0.72 and −0.52 for the south, making them high and moderately correlated, respectively. The dashed lines show the un-weighted linear fit to each hemisphere, clearly showing the anticorrelation.

Downloaded from https://academic.oup.com/mnras/article/438/2/1611/1013156 by guest on 06 May 2025

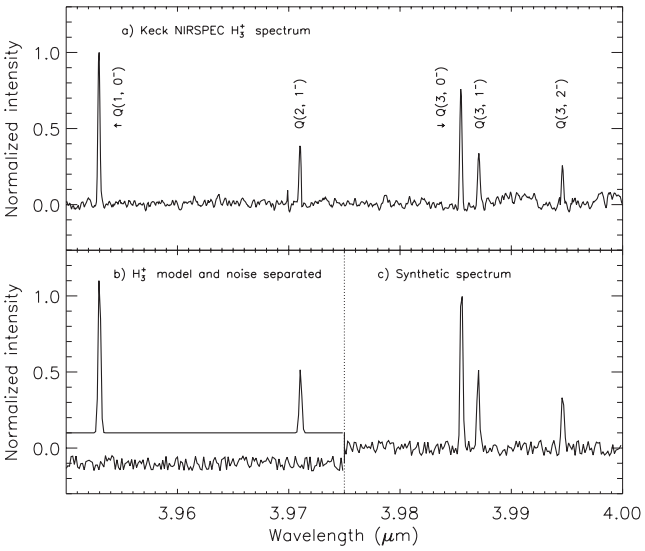

Figure 3. (a) The Keck NIRSPEC H_3^+ spectrum of Saturn's northern aurora, covering 14 min of exposure (7 min on Saturn). The H_3^+ line assignments are indicated, all of which are from the Q-branch ($\Delta J = 0$). This spectrum fits to $T = 528 \pm 17$ K and $N = 1.8 \pm 0.3 \times 10^{15}$ m^{-2}. (b) The H_3^+ spectral model (offset by $+0.1$ in y), and the random noise (offset by -0.1 in y). (c) The two model components combined, comparing well to the actual NIRSPEC observations of (a).

There are 10 H_3^+ spectra for each hemisphere, each covering 14 min, for a total of about two hours of observation, with a wavelength range spanning from 3.95 to 4.0 μm at a spectral resolution of $R = \lambda/\Delta\lambda \sim 25\,000$. An example Keck NIRSPEC H_3^+ spectrum can be seen in Fig. 3(a). The temperature and density spectral fits for all the spectra can be seen in Fig. 2, with errors produced by the fitting program. This region contains, amongst others, the H_3^+ $Q(1, 0^-)$ and $Q(3, 0^-)$ $\nu_2 \rightarrow 0$ vibrational transitions – the intensity per molecule of these lines as a function of temperature can be seen in Fig. 1. See McCall (2001) for more details on the H_3^+ line notations. Since the ratio of the intensity of these two lines changes drastically over the range of temperatures observed at the giant planets, this region has been used in many previous studies to determine the physical conditions of the upper atmospheres of the giant planets (see Miller et al. 2006, and references therein).

The H_3^+ temperature and density of the Keck spectral data of O'Donoghue et al. (2014), shown in Fig. 2, was fitted using Cramer's rule (Bevington & Robinson 2003), applying it to the spectral function described detailed in Section 3. For the 10 sets of observations, the mean northern temperature is 527 K with an average error (as given by Cramer's rule) of 18 K, and a standard deviation of 11 K, whist the average temperature of the south is 583 K with a mean error of 13 K and a standard deviation of 5 K. The H_3^+ column density is moderately higher in the north at 1.6×10^{15} m^{-2} with a mean error of 0.3×10^{15} m^{-2} and a standard deviation of 0.2×10^{15} m^{-2}, whereas in the south the density is 1.2×10^{15} m^{-2} with the mean error and standard deviation both being 0.1×10^{15} m^{-2}. The correlation coefficient in the north is -0.72 with the south being -0.52, suggesting a strong to moderate anticorrelation, respectively.

By virtue of the larger temperatures in the south, emission from that pole is more intense by a factor of 1.5. Therefore, with the same amount of noise present for all spectra, the signal to noise in spectra from the south will have an SNR 1.5 times that of the north. Given the ambiguity in the published literature on how to treat the anticorrelation between H_3^+ temperature and density, it is currently unclear how to fully capture the inherent uncertainties of the two parameters.

3 SYNTHETIC MODEL SPECTRA

In order to investigate what implications the anticorrelation between H_3^+ temperature and density have on the uncertainty on these parameters, we construct a large set of synthetic spectra, at given temperatures and densities, for a range of SNRs, and fit these using our standard fitting routine. We then compare the standard deviation of our fitted parameters to the error produced by the routine. These results can then be applied to interpret the Keck observations of Saturn.

The H_3^+ spectrum, $I(N, T, \lambda)$, can be theoretically treated as a sum of Gaussians, each describing a ro-vibrational transition at a temperature, T, and density, N:

$$I(N, T, \lambda) = N \sum_{l=0}^{\text{all}} I(l, T) \exp \frac{-(\lambda - (\lambda_l + s(\lambda))^2}{2\sigma(\lambda)^2} + b(\lambda), \quad (1)$$

where $I(l, T)$ is the intensity per molecule of ro-vibrational transition l at temperature T, λ_l is the wavelength that transition l emits at, $\sigma(\lambda)$ is the wavelength-dependent spectral line width, $s(\lambda)$ is the wavelength offset between observed and theoretical line wavelengths, and $b(\lambda)$ is a function that describes the background emission upon which the H_3^+ emission is situated. The function $I(l, T)$ is given by the following expression:

$$I(l, T) = \frac{g_l(2J_l + 1)hc\omega_l A_l}{4\pi Q(T)} \exp\left(\frac{-E_l'}{kT}\right), \quad (2)$$

where for each transition l, g_l is the spin degeneracy, J_l is the angular quantum number of the upper level, h is Planck's constant, c is the speed of light, ω_l is the transition frequency, A_l is the Einstein A coefficient for spontaneous emission, $Q(T)$ is the temperature dependent H_3^+ partition function, E_l' is the energy of the upper level and k is Boltzmann's constant. The parameters for the H_3^+ line transitions are obtained from Neale, Miller & Tennyson (1996), and the partition function is given by Miller et al. (2010).

Since $\sigma(\lambda)$, $s(\lambda)$ and $b(\lambda)$ in equation (1) are polynomials that can take, in principle, any number of coefficients (but at least one), the minimum number of free parameters of equation (1) is five (i.e. T, N, σ, s and b), which is the number used here. Several previous studies (e.g. Melin et al. 2007; Lystrup et al. 2008; Melin et al. 2011b,c, 2013; O'Donoghue et al. 2014) have minimized the parameters of equation (1) using Cramer's Rule. This method is outlined in Melin et al. (2013).

Here, a large set of synthetic spectra is generated for temperatures between 400 and 1200 K in steps of 100 K, for a range of SNRs between 3 and 1000. For each synthetic spectrum $b = 0$, $s = 0$ and $\sigma = 10^{-3}$ μm, with 1024 spectral elements (modelled pixels) modelled between 3.95 and 4.00 μm to correspond to the spectral range observed with Keck NIRSPEC (O'Donoghue et al. 2014). For each temperature and SNR combination, 1000 synthetic spectra were created, producing a total of 198 000 spectra used for this study. The column density acts only as a constant multiplier of the intensity, and is here is kept at a constant 10^{16} m^{-2} for all models. Each synthetic spectrum is the sum of the model spectrum and a noise level appropriate to the desired SNR. The model is described by equation (1) and the noise is generated by the IDL *randomu* function. An example of the two components and the resulting synthetic spectrum can be seen in Fig. 3, which also shows

Downloaded from https://academic.oup.com/mnras/article/438/2/1611/1013156 by guest on 06 May 2025

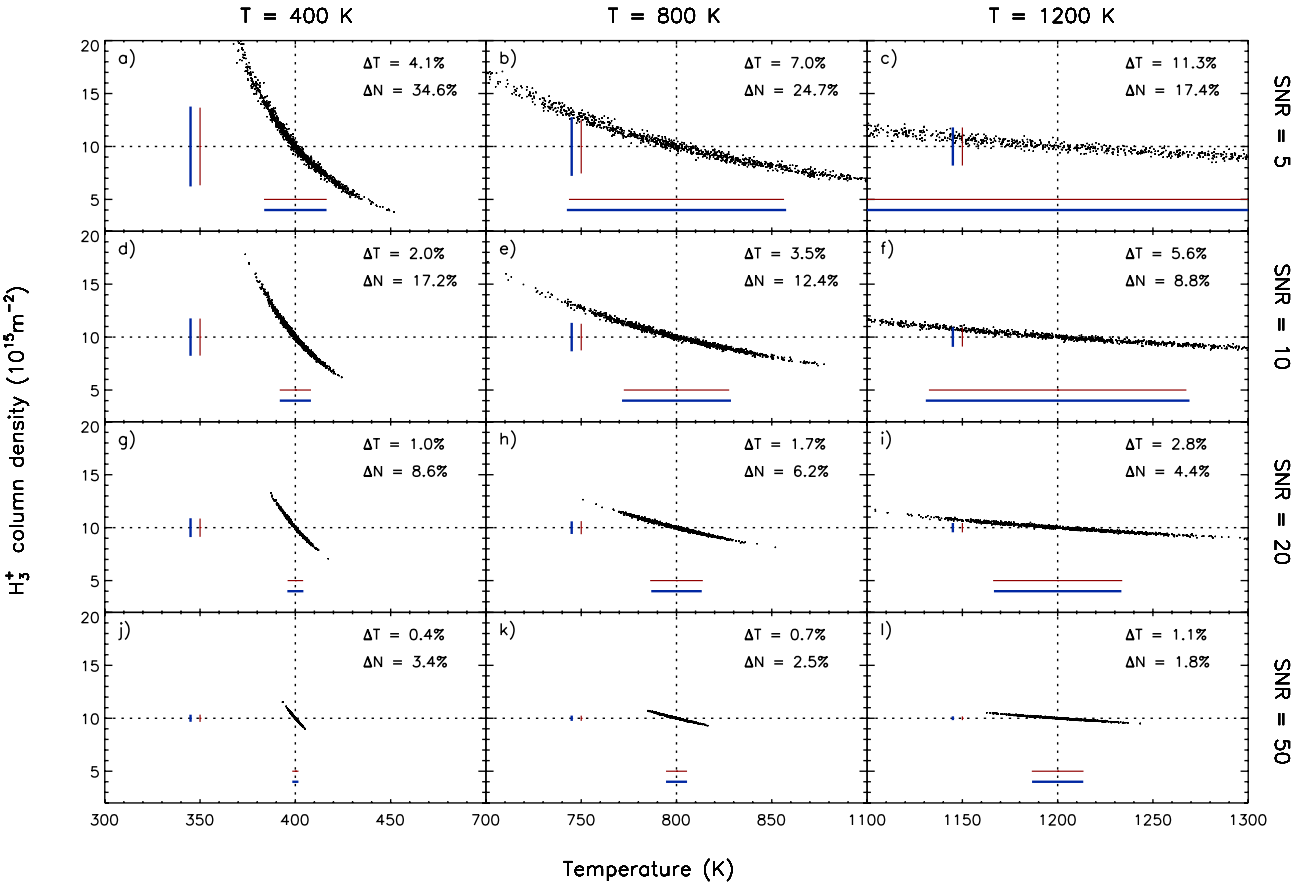

Figure 4. The fitted H_3^+ density as a function of temperature for fixed temperatures of 400, 800 and 1200 K, and for SNRs of 5, 10, 20 and 50. Each plot contains 1000 points, each signifying an individual fit to a synthetic H_3^+ spectrum at temperature T. The bold blue line shows the standard deviation in both temperature (horizontal) and density (vertical) of these fits, and the thin red line shows the average errors on these two parameters, as given by the fitting routine. These two lines are always similar within a few per cent. The percentage error on both parameters is also given. The higher the SNR, the better constrained the H_3^+ temperature and density becomes.

a spectrum obtained by Keck NIRSPEC (from O'Donoghue et al. 2014), for comparison. The synthetic spectrum in Fig. 3(c) compares well to the real spectrum in Fig. 3(a). For this study, a total of 198 000 synthetic spectra are fitted to determine T and N, a large enough sample for us to address the statistical behaviour of the anticorrelation between the H_3^+ temperature and density.

Fig. 4 shows a subset of the model fits, with each plot showing the result of 1000 spectral fits to synthetic spectra at a given temperature and SNR. Tables 1 and 2 show the errors on temperature and density, respectively, for the range of temperatures and SNRs considered here. These errors represent the lower limit that is achievable when fitting H_3^+ Q-branch spectra.

This modelling effort relies on the assumption that LTE applies, an assumption that has been shown to break down at high altitudes at both Jupiter and Saturn (Melin et al. 2005; Tao, Badman & Fujimoto 2011). However, the fundamental $\nu_2 \rightarrow 0$ transitions are the least affected by this (Melin et al. 2005) such that we can assume conditions of *quasi*-LTE (Miller et al. 2006), which is to say that whilst some departures from LTE may exist, the LTE assumption remains valid.

4 RESULTS AND DISCUSSION

For each temperature and SNR, we plot the H_3^+ temperature as a function of density, and compare the mean error of these parameters to the standard deviation of the fitted values. Fig. 4 shows the fitted temperature and density for temperature of 400, 800 and 1200 K, for a range of SNRs of 5, 10, 20 and 50. The thick blue bar shows the standard deviation of the fitted values, while the thin red lines shows the mean error, as provided by the fitting routine.

For each temperature and SNR, a total of 1000 spectra are fitted, and we expect the standard deviation of temperatures and densities to represent the 1σ uncertainty of these parameters. Here, as seen in Fig. 4, we find that the mean errors provided by Cramer's rule are almost identical to the standard deviation on the fitted values – and we conclude that the errors that come out of Cramer's rule fully capture the uncertainty introduced by the interdependence of H_3^+ temperature and density. This is in contrast to the findings of Lam et al. (1997). We do however, note that the H_3^+ total emission parameters formulated by Lam et al. (1997) remains a very useful parameters, signifying the energy lost by radiation to space.

This work suggests that the correlation between H_3^+ temperature and density that exists outside of the error bars observed by Raynaud et al. (2004) and Lam et al. (1997) in the auroral region of Jupiter is real. This may be evidence of either (a) the thermostat effect, where by dense regions of H_3^+ radiate away more energy than less dense ones, or (b) that different altitudes of the ionosphere are sampled, with high-altitude regions being less dense and hotter than lower-altitude regions. Any altitudinal differences in where the H_3^+ emission peak occurs could be driven by the energy of the particle

Downloaded from https://academic.oup.com/mnras/article/438/2/1611/1013156 by guest on 06 May 2025

Table 1. The average error of the H_3^+ temperature, ΔT, in Kelvin, as a function of observed temperature (T) and SNR for all 198 000 synthetic spectra fitted here (1 000 for each temperature and SNR combination).

SNR / $T \rightarrow$	400 K	500 K	600 K	700 K	800 K	900 K	1000 K	1100 K	1200 K
3	27.3	35.6	46.8	67.7	94.2	123.8	158.0	189.8	220.5
4	20.5	26.7	34.9	50.4	70.4	93.4	118.2	142.5	167.6
5	16.4	21.3	27.8	40.3	56.0	74.3	93.5	115.2	135.2
6	13.7	17.8	23.1	33.5	46.4	61.3	78.0	95.0	112.8
7	11.7	15.3	19.8	28.7	39.7	52.4	66.7	81.4	96.7
8	10.2	13.3	17.3	25.1	34.7	45.7	58.3	71.1	84.6
10	8.2	10.6	13.8	20.1	27.7	36.6	46.4	57.0	67.5
12	6.8	8.9	11.5	16.7	23.1	30.5	38.8	47.4	56.4
14	5.8	7.6	9.9	14.3	19.8	26.1	33.1	40.6	48.3
16	5.1	6.6	8.6	12.5	17.3	22.8	29.0	35.6	42.2
18	4.5	5.9	7.7	11.1	15.4	20.3	25.7	31.6	37.6
20	4.1	5.3	6.9	10.0	13.8	18.3	23.2	28.4	33.8
25	3.3	4.2	5.5	8.0	11.0	14.6	18.5	22.7	27.1
30	2.7	3.5	4.6	6.7	9.2	12.2	15.4	19.0	22.6
35	2.3	3.0	4.0	5.7	7.9	10.4	13.2	16.2	19.3
40	2.0	2.7	3.5	5.0	6.9	9.1	11.6	14.2	16.9
50	1.6	2.1	2.8	4.0	5.5	7.3	9.3	11.4	13.5
75	1.1	1.4	1.8	2.7	3.7	4.9	6.2	7.6	9.0
100	0.8	1.1	1.4	2.0	2.8	3.6	4.6	5.7	6.8
250	0.3	0.4	0.6	0.8	1.1	1.5	1.9	2.3	2.7
500	0.2	0.2	0.3	0.4	0.6	0.7	0.9	1.1	1.4
1000	0.1	0.1	0.1	0.2	0.3	0.4	0.5	0.6	0.7

Table 2. The percentage error of the H_3^+ column integrated density, ΔN, as a function of observed temperature (T) and SNR.

SNR / $T \rightarrow$	400 K	500 K	600 K	700 K	800 K	900 K	1000 K	1100 K	1200 K
3	58.4	47.0	40.9	41.7	41.6	40.5	37.7	34.6	31.1
4	43.4	35.1	30.7	31.1	31.0	30.0	28.0	25.7	22.6
5	34.6	28.0	24.5	24.9	24.7	23.9	22.5	20.2	17.4
6	28.8	23.4	20.5	20.7	20.6	20.0	18.6	16.9	14.7
7	24.6	20.1	17.5	17.8	17.7	17.1	16.0	14.5	12.6
8	21.5	17.5	15.3	15.5	15.5	15.0	14.0	12.8	11.0
10	17.2	14.0	12.3	12.4	12.4	11.9	11.2	10.1	8.8
12	14.3	11.7	10.2	10.4	10.3	9.9	9.3	8.5	7.3
14	12.3	10.0	8.8	8.9	8.8	8.5	8.0	7.2	6.3
16	10.7	8.8	7.7	7.8	7.7	7.5	7.0	6.3	5.5
18	9.5	7.8	6.8	6.9	6.9	6.6	6.2	5.6	4.9
20	8.6	7.0	6.1	6.2	6.2	6.0	5.6	5.1	4.4
25	6.9	5.6	4.9	5.0	5.0	4.8	4.5	4.1	3.5
30	5.7	4.7	4.1	4.1	4.1	4.0	3.7	3.4	2.9
35	4.9	4.0	3.5	3.5	3.5	3.4	3.2	2.9	2.5
40	4.3	3.5	3.1	3.1	3.1	3.0	2.8	2.5	2.2
50	3.4	2.8	2.5	2.5	2.5	2.4	2.2	2.0	1.8
75	2.3	1.9	1.6	1.7	1.7	1.6	1.5	1.4	1.2
100	1.7	1.4	1.2	1.2	1.2	1.2	1.1	1.0	0.9
250	0.7	0.6	0.5	0.5	0.5	0.5	0.4	0.4	0.4
500	0.3	0.3	0.2	0.2	0.2	0.2	0.2	0.2	0.2
1000	0.2	0.1	0.1	0.1	0.1	0.1	0.1	0.1	0.1

precipitating, depositing their energy at different altitudes (Galand et al. 2011; Tao et al. 2011).

In practical terms, one can effectively increase the SNR by increasing the integration-time for each spectrum. This would have the effect of decreasing the error bars on both the temperature and density, revealing parameters closer to those that truly characterize the ionosphere system. If an anticorrelation is still observed within a sequence of high SNR H_3^+ spectra, then this could be evidence for H_3^+ acting as a thermostat, effectively radiating energy away from the planet.

Fig. 4 shows that the uncertainties on the H_3^+ temperature and density are not constant for different temperatures observed at the same SNR, and that the nature of the anticorrelation is a function of temperature. At 1200 K, the percentage error on the density is smaller than at 400 K, whilst the percentage error on the temperature is larger by about a factor of 2. In addition, the slope of the

Downloaded from https://academic.oup.com/mnras/article/438/2/1611/1013156 by guest on 06 May 2025

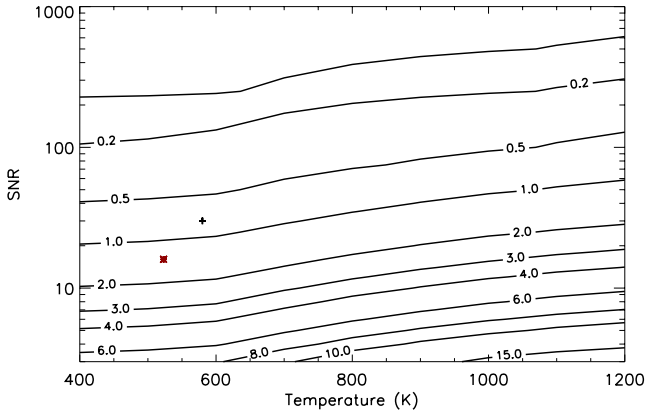

Figure 5. The percentage error of the H_3^+ temperature ($\Delta T/T$) as a function of SNR and fitted temperature. The black cross and the red star show the southern and northern aurora of Fig. 2, respectively.

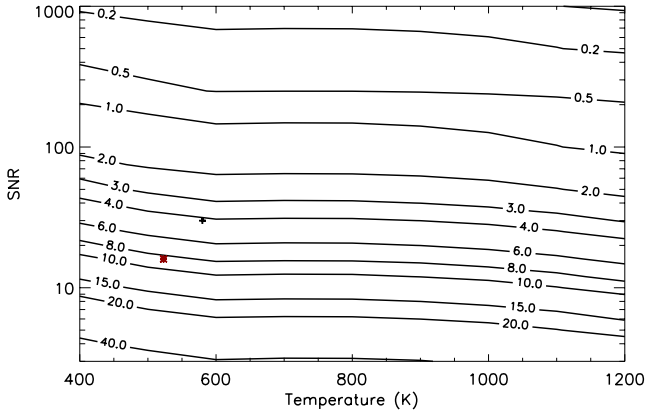

Figure 6. As Fig. 5 but showing the percentage error on the H_3^+ column density ($\Delta N/N$).

anticorrelation curve (dots) becomes steeper as the temperature goes up. Additionally, as seen in Table 1, in order to achieve a temperature error of $\Delta T = 10$ K at 400 K requires an SNR of 8, whist at 1200 K, an SNR of ∼75 is required. This highlights the curious effect by which the H_3^+ temperature at Saturn can be constrained better than at Jupiter and Uranus, despite lower SNR, only by virtue of being cooler.

Fig. 5 shows the percentage uncertainty of the H_3^+ temperature as a function of SNRs and fitted temperature. The uncertainty increases for a constant SNR as the temperature increases with the error at 400 K being about three times smaller than at 1200 K. This is because the rate of change of intensity between the H_3^+ lines within our spectral region in Fig. 3 is smaller at 1200 K than at 400 K – this can be seen in Fig. 1.

Fig. 6 shows the percentage error on the H_3^+ density as a function of SNR and temperature. This error is larger, almost by a factor of 10, than the percentage error on the temperature seen in Fig. 5. This is because whilst the temperature drives the intensity exponentially, the intensity is only a linear function of density, making the density parameter more poorly constrained.

There are more sources of uncertainty than the one related to the anticorrelation of H_3^+ temperature and density detailed here. For example, if the flux calibration spectrum, generally derived from observations of an A0 star, is poorly constrained, then the uncertainty in the column density will have increased significantly over that of the temperature. This is because over relatively narrow wavelength regions, the flux calibration is a constant multiplier and does not affect the relative intensities of the H_3^+ lines – this is shown in Melin et al. (2013) for Gemini Near InfraRed Spectrograph (GNIRS) observations of Uranus obtained under non-optimal sky conditions. These additional errors must be properly accounted for, but are not considered in this study.

Both Figs 5 and 6 have the mean northern and southern observations of Saturn's aurora of O'Donoghue et al. (2014) indicated, agreeing well with the observed SNR of these spectra, with an inferred SNR of about 18 for the northern aurora and about 30 for the southern aurora. This is consistent with the fact that the southern aurora is more intense than the north than the by a factor of 1.5, mainly driven by the higher temperatures.

The observations of O'Donoghue et al. (2014) seen in Fig. 2 have errors of a similar magnitude to the variability of values observed within each hemisphere. Therefore, with the errors retrieved Cramer's rule representing the true standard deviation of the fitted parameters, the observed variability cannot be said to be statistically significant. However, the difference in temperature between the two hemispheres can clearly be said to be physical. This hemispheric temperature difference is striking and is discussed in more detail in O'Donoghue et al. (2014).

Tao et al. (2011, 2012) showed that the primary energy and energy flux of the particle precipitation could theoretically be derived by comparing the intensity of different H_3^+ spectral lines, requiring a minimum SNR of about 100 for each line. Table 1 shows that at 1000 K, the inherent interdependence of H_3^+ temperature and density would produce a temperature error of about a 6.8 K (0.7 per cent), whereas Table 2 shows that the H_3^+ density would be constrained within 0.9 per cent. This suggests that the H_3^+ anticorrelation does not impose additional limits to the technique outlined by Tao et al. (2012).

The work undertaken here models the fundamental *Q*-branch emission around 4 μm, to match the spectral window of Keck NIRSPEC. The *R*-branch can be found shortward of this (∼3.5 μm), and has also been used to determine the temperatures of the upper atmospheres. At the temperature range considered here (400 to 1200 K), the $Q(1, 0^-)$ and $Q(3, 0^-)$ provide the largest change in ratio, and we expect the error on the temperature derived from *R*-branch emission to produce larger temperatures. Therefore, the modelling effort presented here provides lower limits on H_3^+ temperature and density errors, expressed as a function of SNR and temperature. The *P*-branch spectrum of H_3^+, at longward wavelengths of *Q*, is not visible from the ground, as it coincides with broad-bands of absorption in our own atmosphere. However, with space-based platforms not suffering these constraints, this emission has been observed at low-spectral resolution at both Jupiter and Saturn (e.g. Badman et al. 2011).

5 SUMMARY

Our findings can be summarized as follows:

(i) In contrast to Lam et al. (1997) we find that the uncertainties produced by the H_3^+ fitting routine (invoking Cramer's rule) do truly represent the physical uncertainty of the fitted temperature and density, accounting fully for the anticorrelation. This means that variability outside of these uncertainties, providing that there are no additional external sources of error, is statistically deemed to be physical in nature, even when this variability is in the form of a strong anticorrelation.

Downloaded from https://academic.oup.com/mnras/article/438/2/1611/1013156 by guest on 06 May 2025

(ii) The fractional uncertainty on the temperature for a given SNR increases with temperature, whereas the fractional uncertainty of the density decreases slightly.

(iii) We derive the minimum error on the H_3^+ temperature and density that is achievable when fitting H_3^+ spectra – seen in Table 1, which can be used to attribute errors to H_3^+ temperatures derived via alternative methods, e.g. by direct line ratios (e.g. Stallard et al. 2002).

(iv) There is not enough statistical confidence to distinguish the variability of each pole of Saturn observed by O'Donoghue et al. (2014), outside the level of uncertainty. However, the difference between each hemisphere, both in H_3^+ temperature and density, can be considered to be physical. This indicates that the two hemispheres are subject to different heating injected via the magnetosphere–ionosphere–thermosphere interaction (Badman et al. 2011).

ACKNOWLEDGEMENTS

The data presented herein were obtained at the W.M. Keck Observatory, which is operated as a scientific partnership among the California Institute of Technology, the University of California and NASA. Discussions within the international team lead by Tom Stallard on 'Comparative Jovian Aeronomy' have greatly benefited this work, hosted by the International Space Science Institute (ISSI). This work was supported by a RCUK Fellowship for TSS, by the UK STFC for HM, a Royal Astronomical Society Research Fellowship for SVB, and at SET by NASA CDAP grant NNX13AG41G. JO'D and JSDB were supported by STFC studentships. The authors thank an anonymous reviewer for helpful comments and suggestions.

REFERENCES

Badman S. V., Tao C., Grocott A., Kashahara S., Melin H., Brown R. H., Baines K. H., Fujimoto M., Stallard T., 2011, Icarus, 216, 367
Bevington P. R., Robinson D. K., in Bevington P. R., Robinson K. D., eds, 2003, Data Reduction and Error Analysis for the Physical Sciences. McGraw-Hill, Boston, MA
Cowley S. W. H., Bunce E. J., 2003, Ann. Geophys., 21, 1691
Drossart P. et al., 1989, Nature, 340, 539
Feuchtgruber H., Encrenaz T., 2003, A&A, 403, L7
Galand M., Moore L., Mueller-Wodarg I., Mendillo M., Miller S., 2011, J. Geophys. Res. (Space Phys.), 116, A09306
Geballe T. R., Oka T., 1996, Nature, 384, 334
Koskinen T. T., Aylward A. D., Miller S., 2007, Nature, 450, 845
Lam H. A., Achilleos N., Miller S., Tennyson J., Trafton L. M., Geballe T. R., Ballester G. E., 1997, Icarus, 127, 379
Lystrup M. B., Miller S., Dello Russo N., Vervack R. J., Jr, Stallard T., 2008, ApJ, 677, 790
McCall B. J., Geballe T. R., Hinkle K. H., Oka T., 1999, ApJ, 522, 338
McCall B. J., 2001, PhD thesis, Univ. Chicago
McLean I. S. et al., 1998, in Fowler A. M., ed., Proc. SPIE Conf. Ser., Vol. 3354, Infrared Astronomical Instrumentation. SPIE, Bellingham, p. 566
Melin H., Miller S., Stallard T., Grodent D., 2005, Icarus, 178, 97
Melin H., Miller S., Stallard T., Smith C., Grodent D., 2006, Icarus, 181, 256
Melin H., Miller S., Stallard T., Trafton L. M., Geballe T. R., 2007, Icarus, 186, 234
Melin H. et al., 2011a, Geophys. Res. Lett., 381, L15203
Melin H., Stallard T., Miller S., Lystrup M. B., Trafton L. M., Booth T. C., Rivers C., 2011b, MNRAS, 410, 641
Melin H., Stallard T., Miller S., Trafton L. M., Encrenaz T., Geballe T. R., 2011c, AJ, 729, 134
Melin H., Stallard T. S., Miller S., Geballe T. R., Trafton L. M., O'Donoghue J., 2013, Icarus, 223, 741
Miller S. et al., 2000, Adv. Space Res., 26, 1477
Miller S., Stallard T., Smith C. et al., 2006, Phil. Trans. R. Soc. A, 364, 3121
Miller S., Stallard T., Melin H., Tennyson J., 2010, Faraday Discussions, 147, 283
Neale L., Miller S., Tennyson J., 1996, ApJ, 464, 516
O'Donoghue J., Stallard T. S., Melin H., Jones G. H., Cowley S. W. H., Miller S., Baines K. H., Blake J. S. D., 2013, Nature, 496, 193
O'Donoghue J. et al., 2014, Icarus, 229, 214
Oka T., 1980, Phys. Rev. Lett, 45, 531
Raynaud E., Lellouch E., Maillard J.-P., Gladstone G. R., Waite J. H., Bézard B., Drossart P., Fouchet T., 2004, Icarus, 171, 133
Stallard T., Miller S., Millward G., Joseph R. D., 2002, Icarus, 156, 498
Stallard T. S. et al., 2012, Phil. Trans. R. Soc. A, 370, 5213
Tao C., Badman S. V., Fujimoto M., 2011, Icarus, 213, 581
Tao C., Badman S. V., Uno T., Fujimoto M., 2012, Icarus, 221, 236
Tyler G. L. et al., 1986, Science, 233, 79
Tyler G. L. et al., 1989, Science, 246, 1466

This paper has been typeset from a TEX/LATEX file prepared by the author.

Downloaded from https://academic.oup.com/mnras/article/438/2/1611/1013156 by guest on 06 May 2025